

## Accepted Article

**Title:** Tuning the Circular Dichroism and Circular Polarized Luminescence Intensities of Chiral 2D Hybrid Organic-Inorganic Perovskites through Halogenation of the Organic Ions

**Authors:** Jin-Tai Lin, Deng-Gao Chen, Lan-Sheng Yang, Tai-Chun Lin, Yi-Hung Liu, Yu-Chiang Chao, Pi-Tai Chou, and Ching-Wen Chiu

This manuscript has been accepted after peer review and appears as an Accepted Article online prior to editing, proofing, and formal publication of the final Version of Record (VoR). This work is currently citable by using the Digital Object Identifier (DOI) given below. The VoR will be published online in Early View as soon as possible and may be different to this Accepted Article as a result of editing. Readers should obtain the VoR from the journal website shown below when it is published to ensure accuracy of information. The authors are responsible for the content of this Accepted Article.

**To be cited as:** *Angew. Chem. Int. Ed.* 10.1002/anie.202107239

**Link to VoR:** <https://doi.org/10.1002/anie.202107239>

## RESEARCH ARTICLE

# Tuning the Circular Dichroism and Circular Polarized Luminescence Intensities of Chiral 2D Hybrid Organic-Inorganic Perovskites through Halogenation of the Organic Ions

Jin-Tai Lin,<sup>1, ξ</sup> Deng-Gao Chen,<sup>1, ξ</sup> Lan-Sheng Yang,<sup>2</sup> Tai-Chun Lin,<sup>1</sup> Yi-Hung Liu,<sup>3</sup> Yu-Chiang Chao,<sup>\*, 2</sup> Pi-Tai Chou,<sup>\*, 1,4</sup> and Ching-Wen Chiu<sup>\*, 1</sup>

Dedication ((optional))

**Abstract:** By incorporating various halogen (F, Cl, Br, and I)-substituted chiral organic cations, the effects of chiral molecules on chiroptical properties of hybrid organic inorganic perovskite (HOIP) are investigated. Among them, the HOIP having Cl-substituted chiral cation exhibits the highest circular dichroism (CD) and circular polarized luminescence (CPL) intensities, indicating the existence of the largest rotatory strength, whereas the F-substituted one shows the weakest intensities. The observed modulation can be correlated to the varied magnetic transition dipole of HOIPs, which is sensitive to the d-spacing between inorganic layers and the halogen-halogen interaction between organic cations and the inorganic sheets. Although a larger angular momentum of organic cation is expected as the atomic number of the *para*-substituent increases, the simultaneous increase in atom size enlarges the d-spacing of the HOIPs, thereby lowering the magnetic transition dipole. However, the strong halogen-halogen interaction existing in Cl-substituted system leads to a significantly increased rotational strength. These offsetting effects meet the optimal CD and CPL intensity with chlorine substitution, rendering the rotatory strength of HOIPs arranged in the order of (CIMBA)<sub>2</sub>PbI<sub>4</sub>>(BrMBA)<sub>2</sub>PbI<sub>4</sub>>(IMBA)<sub>2</sub>PbI<sub>4</sub>>(MBA)<sub>2</sub>PbI<sub>4</sub>>(FMBA)<sub>2</sub>PbI<sub>4</sub>. The modulation of the magnetic transition dipoles of HOIP paves the new avenue for designing hybrid perovskite-based spintronic devices.

## Introduction

Hybrid organic-inorganic perovskites (HOIPs) have revolutionized the field of solution-processable optoelectronic devices owing to their long-range charge carrier diffusion

lengths,<sup>[1]</sup> high dielectric constants,<sup>[2]</sup> as well as tunable optical absorption and emission wavelengths.<sup>[3]</sup> Accordingly, HOIPs have found numerous applications in solar cells,<sup>[4]</sup> light-emitting diodes (LEDs)<sup>[5]</sup> and field-effect transistors (FETs).<sup>[6]</sup> In addition to their superb solar-electric conversion efficiency, the intrinsic strong spin-orbital coupling,<sup>[7]</sup> large Rashba splitting<sup>[8]</sup> and magneto-photoluminescence response<sup>[9]</sup> have rendered HOIPs promising candidates for electronic and spintronic device.<sup>[10]</sup> Moreover, in recent years, chiral-perovskites with non-centrosymmetric property have been widely investigated due to its ferroelectricity, circular dichroism (CD) and circular polarized photoluminescence (CPL) responses, which have been regarded as promising materials in chiroptoelectronics.<sup>[11]</sup> Among them, polarized absorption (CD) and photoluminescence (CPL) responses arise from asymmetric absorption/emission rates of left-handed polarized and right-handed polarized lights according to different Einstein coefficients.<sup>[12]</sup> Thence, the observed CD/CPL responses imply asymmetric absorption/emission rates between electron spin up and spin down species, which follows the selection rule in spin polarized absorption/emission.<sup>[9b, 13]</sup> To be more specific, the efficient spin filtering created by chiral molecules allows nanoscale manipulation of quantum spins, a process that is critical for spintronic or chiroptoelectronic applications. Therefore, the chiroptoelectronic device featuring chiral HOIPs brings the perovskite materials to an intensively sought-after field.<sup>[11, 14]</sup>

In 2006, Billing's group reported the first chiral two-dimensional (2D) perovskite by introducing either *R*- or *S*-form methyl-benzyl ammonium (MBA) ion to lead iodide perovskite.<sup>[15]</sup> However, not until 2017 were the chiroptical properties of these two chiral HOIPs investigated with CD by Moon's group.<sup>[16]</sup> In the following year, spin-polarized photoluminescence of chiral HOIPs was observed in the absence of an external magnetic field.<sup>[9b]</sup> Since then, the chiroptical properties of chiral HOIPs featuring various metal ions, including lead,<sup>[17]</sup> tin,<sup>[14c]</sup> copper<sup>[18]</sup> and bismuth/silver system<sup>[14d]</sup> have been investigated. However, most of these studies focus on chiral MBA-based perovskites to probe their chiroptical properties. A comprehensive understanding of the influence of the chiral organic cation on the chiroptical properties of HOIPs remains unexplored.

Like a pair of enantiomers, circular polarization of transmitted light exerted by a chiral HOIP built with *R*-form MBA results in optical rotatory dispersion (ORD) curves in the CD spectrum with opposite sign and equal strength to its *S*-form counterpart.<sup>[14b, 17]</sup>

[1] J.-T. Lin, D.-G. Chen, T.-C. Lin, P.-T. Chou, C.-W. Chiu  
Department of Chemistry, National Taiwan University, Taipei, 10617 Taiwan.

E-mail: [cwchiu@ntu.edu.tw](mailto:cwchiu@ntu.edu.tw)

E-mail: [chop@ntu.edu.tw](mailto:chop@ntu.edu.tw)

[2] L.-S. Yang, Y.-C. Chao  
Department of Physics, National Taiwan Normal University, Taipei 116, Taiwan.

E-mail: [ycchao@ntnu.edu.tw](mailto:ycchao@ntnu.edu.tw)

[3] Y.-H. Liu  
Instrumentation Center, National Taiwan University, Taipei 10617 Taiwan.

[4] P.-T. Chou  
Center for Emerging Materials and Advanced Devices, National Taiwan University, Taipei, 10617 Taiwan.

[ξ] equal contribution

## RESEARCH ARTICLE

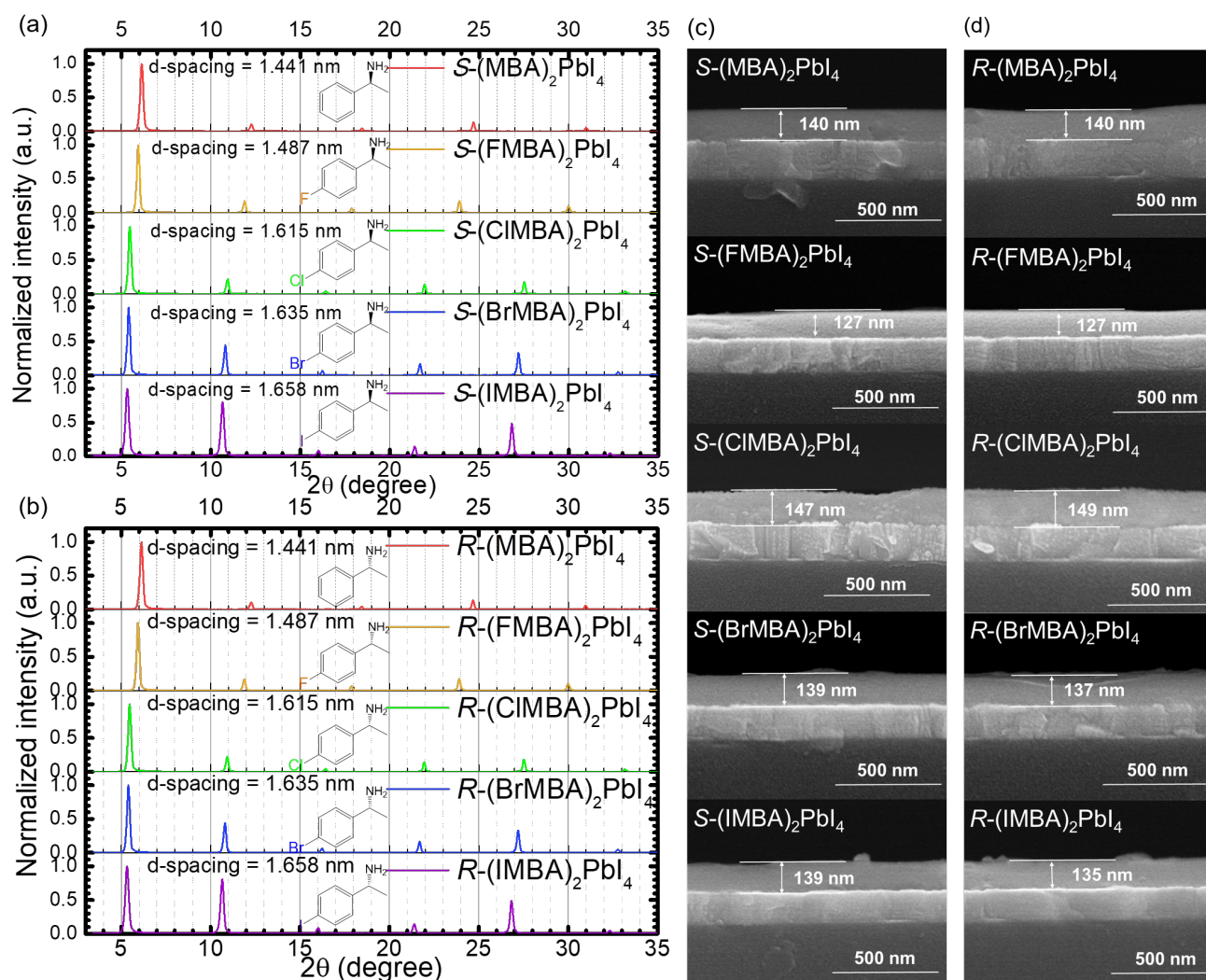


**Figure 1.** (a) XRD pattern of all the fabricated (a) S-form and (b) R-form HOIPs films as depicted in the figure. SEM cross-section images of all the fabricated (c) S-form and (d) R-form HOIPs films. Note that the estimated thicknesses are recorded in the figure.

The same spectral features are also captured in the CPL spectra of a pair of chiral HOIPs.<sup>[14b, 19]</sup> As the ability of a material to induce strong spin polarization of light is critical for effective chiroptoelectronic applications, we herein demonstrate how to manipulate spin polarization of chiral HOIPs through functionalization of the chiral ammonium ion.

As circularly polarized light passes an optically active material (i.e. chiral HOIPs), the CD signals can be obtained from the difference in absorption coefficient ( $\Delta\varepsilon$ ) between left- and right-handed light,<sup>[14d, 20]</sup> and the intensity of CD signal can be illustrated with rotatory strength as depicted in eq. (1):

$$R_{exp} = \frac{3hc10^3 \ln(10)}{32\pi^3 N_A} \int \frac{\Delta\varepsilon}{\nu} d\nu \quad \text{eq. (1)}$$

where  $R$  represents the rotatory strength of the electronic transition between two electronic states and  $\Delta\varepsilon$  denotes the absorption coefficient difference.<sup>[20b]</sup> The equation reveals a positive correlation between the rotatory strength and the intensity of CD signal. Furthermore, the circular polarization luminosity in CPL spectra was also found to be proportional to the rotatory strength.<sup>[21]</sup> Thus, the rotatory strength of the HOIPs can be

investigated experimentally by both CD and CPL spectra from the absorption and emission spectra of HOIPs, respectively. On the other hand, rotatory strength can be determined theoretically from the scalar product between the electric transition dipole moment ( $\hat{M}_{(elec. dipole)}$ ) and the magnetic transition dipole moment ( $\hat{M}_{(mag. dipole)}$ ) of the system as depicted in eq. (2):<sup>[20a]</sup>

$$R_{theo} = \frac{1}{2mc} \text{Im} \int \Psi_g \hat{M}_{(elec. dipole)} \Psi_e d\tau \cdot \int \Psi_g \hat{M}_{(mag. dipole)} \Psi_e d\tau \quad \text{eq. (2)}$$

The derivation originated from the linear displacement of the excited electron when the electric field of the incident light interacts with the molecule. In the meantime, the magnetic field of the excitation source leads to a circulation of the electron, bring both translational and rotatory motions to the excited electron simultaneously.<sup>[20a, 20b]</sup> In short, chiroptical properties such as CD or CPL intensity should be harnessed by the electric and magnetic transition dipole moments of the target material.<sup>[22]</sup> In this work, we measure the chiroptical properties of a series of chiral HOIPs, featuring different halogen-substituted MBA derivatives as the chiral organic spacers, and demonstrate that the intensity of CD

## RESEARCH ARTICLE

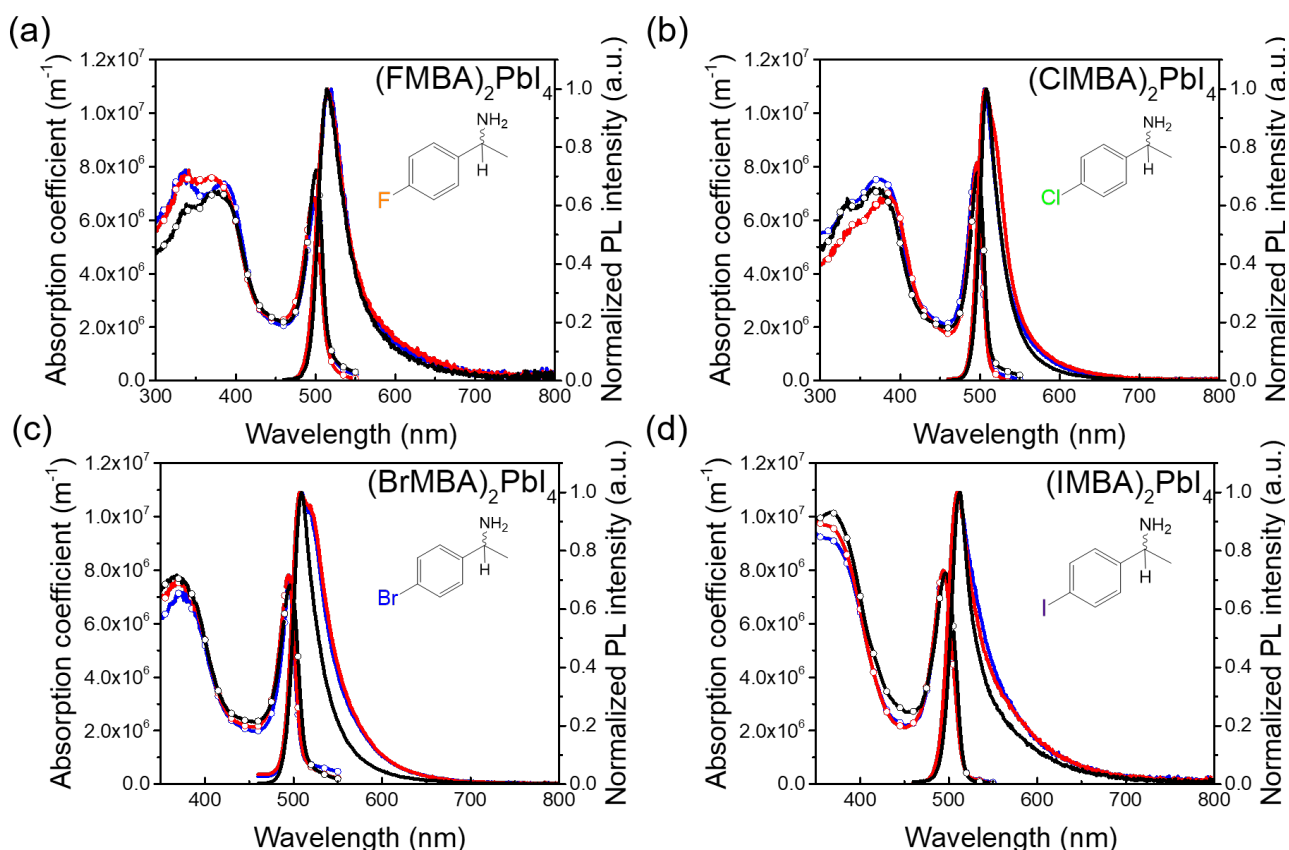


**Figure 2.** (a) The absorption (solid circle line) and normalized photoluminescence (PL, solid line) spectra of the fabricated *R*- (blue), *S*- (red) and *rac*- (black) HOIPs films including (a) (FMBA)<sub>2</sub>PbI<sub>4</sub>, (b) (CIMBA)<sub>2</sub>PbI<sub>4</sub>, (c) (BrMBA)<sub>2</sub>PbI<sub>4</sub> and (d) (IMBA)<sub>2</sub>PbI<sub>4</sub> series as depicted in the figure, respectively. (e) Schematic energy diagram of HOIPs.

and CPL signal can be harnessed by the chiral organic cations in a systematic manner.

## Results and Discussion

Prior to investigating the chiroptical properties of HOIPs, a suitable selection of the chiral organic ligands is indispensable. To avoid optical variation resulted from the structural disturbance of the inorganic layers, we decided to focus on the derivatives of MBA with halogen-substitution at the *para*-position of the phenyl group.<sup>[23]</sup> These derivatives included 1-(4-fluorophenyl)ethanamine (FMBA), 1-(4-chlorophenyl)ethanamine (CIMBA), 1-(4-bromophenyl)ethanamine (BrMBA), and 1-(4-iodophenyl)ethanamine (IMBA). For a fair comparison, in addition to the enantiopure *R*- and *S*-form derivatives, HOIPs obtained from the racemic mixture were also prepared. These chiral HOIPs are then named according to the chirality of the organic cation used. For example, (*R*-FMBA)<sub>2</sub>PbI<sub>4</sub>, (*S*-FMBA)<sub>2</sub>PbI<sub>4</sub>, and (*rac*-FMBA)<sub>2</sub>PbI<sub>4</sub> represent respectively the HOIP prepared from *R*-FMBA, *S*-FMBA, and the racemic mixture of FMBA (see **Supporting Information** for details of synthetic routes).

Before discussing the chiroptical spectra of the chiral HOIPs, we have confirmed that all materials adopt layered structure with chiral ammonium ions sitting in between lead-iodide sheets by powder X-ray diffraction (PXRD) and scanning electron

microscope (SEM). As shown in **Figure 1a-b** (see **Figure S15** for *Rac*-forms XRD), all the HOIPs exhibit a set of strong *00l* reflections, demonstrating a layered 2D perovskite structure composed of an inorganic framework and organic layers. It is worth noting that the  $2\theta$  angle of the *001* reflection patterns decreases sequentially from (MBA)<sub>2</sub>PbI<sub>4</sub> (6.13°) to (IMBA)<sub>2</sub>PbI<sub>4</sub> (5.32°). Correspondingly, the estimated *d*-spacing of the HOIP films are in the order of 1.441 nm ((MBA)<sub>2</sub>PbI<sub>4</sub>) < 1.487 nm ((FMBA)<sub>2</sub>PbI<sub>4</sub>) < 1.615 nm ((CIMBA)<sub>2</sub>PbI<sub>4</sub>) < 1.635 nm ((BrMBA)<sub>2</sub>PbI<sub>4</sub>) < 1.658 nm ((IMBA)<sub>2</sub>PbI<sub>4</sub>), which is consistent with the atomic size of the *para*-substituent, implying successful incorporation of these chiral cations. Also, the reflection patterns are independent of the chirality of the cation (*R*- or *S*-form). Apart from this, SEM cross-sectional images (see **Figure 1c-d**) reveal that the thicknesses of the fabricated HOIP films are independent of the *para*-substituents for both *R*- and *S*-forms. Thus, the observed difference in the chiroptical spectra of chiral HOIPs should arise from their intrinsic properties rather than the film thickness.

The absence of significant variation in both the I-Pb-I angle and film thickness was further corroborated by the absorption and photoluminescence spectra of the HOIPs shown in **Figure 2a-d** and **Figure S18** (see **Figure S18** for (MBA)<sub>2</sub>PbI<sub>4</sub>). In all cases, the title HOIPs exhibit a sharp absorption peak at 497 nm and an emission peak at 515 nm, which are similar to those previously reported for (MBA)<sub>2</sub>PbI<sub>4</sub>.<sup>[14b]</sup> Notably, the comparable bandgaps

## RESEARCH ARTICLE

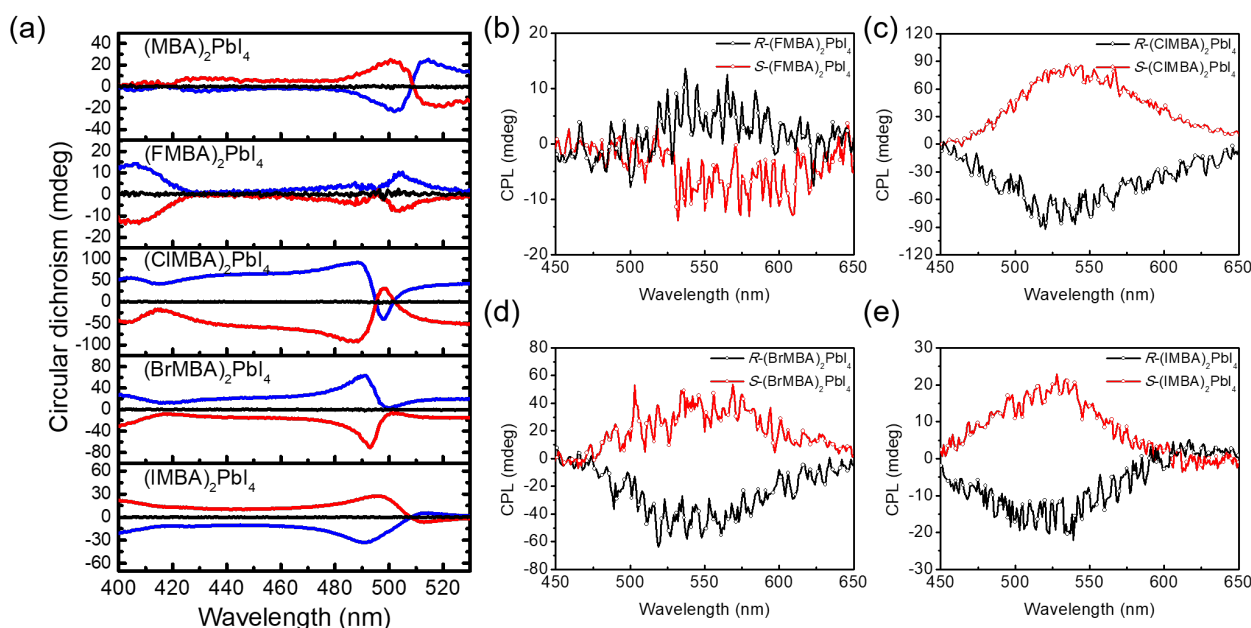


**Figure 3.** (a) CD spectra of the *R*- (blue), *S*- (red) and *rac*- (black) fabricated HOIPs films including (MBA)<sub>2</sub>PbI<sub>4</sub>, (FMBA)<sub>2</sub>PbI<sub>4</sub>, (CIMBA)<sub>2</sub>PbI<sub>4</sub>, (BrMBA)<sub>2</sub>PbI<sub>4</sub> and (IMBA)<sub>2</sub>PbI<sub>4</sub> series as depicted in the figure. Circular polarized photoluminescence (CPL) spectra of the *R*-form (black) and *S*-form (red) fabricated films (b) (FMBA)<sub>2</sub>PbI<sub>4</sub> (c) (CIMBA)<sub>2</sub>PbI<sub>4</sub> (d) (BrMBA)<sub>2</sub>PbI<sub>4</sub> and (e) (IMBA)<sub>2</sub>PbI<sub>4</sub>.

of the chiral HOIPs prepared suggest that the influence of the *para*-substituent of the ammonium cation on the structure of the [PbI<sub>4</sub>]<sup>2-</sup> layer is negligible.<sup>[23]</sup> Thus, any observed variation in chiroptical properties of the title HOIPs caused by structural deformation of the inorganic part can be minimized. More importantly, the value of squared  $\hat{M}_{(elec. dipole)}$  possesses a positive correlation with the absorption coefficient expressed in eq. (3):<sup>[24]</sup>

$$\int \epsilon d\lambda \propto \left| \hat{M}_{(elec. dipole)} \right|^2 \quad \text{eq. (3)}$$

Combining the SEM cross-sectional images (see **Figure 1c-d**), the absorption coefficient of individual HOIP can be estimated by dividing the measured absorbance by the film thickness. Accordingly, all the HOIPs films exhibit a similar absorption coefficient of  $7.80 \times 10^6 \text{ m}^{-1}$  affirming that all chiral HOIPs have comparable intrinsic electric transition dipole moments. Therefore, any chiroptical property changes could be ascribed to the change in the magnetic transition dipole moment of the perovskite induced by the chiral ammonium cation.

By incorporating the chiral organics into HOIPs, all the fabricated films exhibit spin-polarized absorptions in the visible region ranging from 400 to 530 nm as illustrated in **Figure 3a**. Note that the absorption bands of MBA salt derivatives are centered around 275 nm (see **Figure S19** for the absorption spectra of the organic salts); the observed CD absorption in the visible region of the chiral HOIPs should be viewed as an optical response originating from the inorganic layers of HOIPs. Hence, the detection of CD response in the visible region implies that the chirality of the organic cations is successfully transferred to the perovskite inorganic quantum sheets. In terms of the chiroptical properties, the varied CD intensities are of particular interest. The non-substituted chiral MBA perovskite film (i.e. (*R*-MBA)<sub>2</sub>PbI<sub>4</sub> and (*S*-MBA)<sub>2</sub>PbI<sub>4</sub>) exhibit a maxima CD value around 20 mdeg, which is comparable to the previous report.<sup>[17]</sup> However, the maxima CD

intensity of HOIPs dropped to 10 mdeg when the *para*-hydrogen atom of MBA ligand was substituted by a fluorine atom ((FMBA)<sub>2</sub>PbI<sub>4</sub>). Interestingly, a CD intensity value of 90 mdeg was observed in the (CIMBA)<sub>2</sub>PbI<sub>4</sub> series and decreased to 60 and 30 mdeg in the (BrMBA)<sub>2</sub>PbI<sub>4</sub> and (IMBA)<sub>2</sub>PbI<sub>4</sub> series, respectively. The CD results clearly showed that the magnitude of the magnetic transition dipole moments ( $\hat{M}_{(Mag. dipole)}$ ) of HOIPs is strongly dependent on the chiral organic cation.

A related dimensionless *g*-factor spectrum can be derived from the CD spectrum of HOIP. The *g*-factor was obtained by dividing the differential absorbance of the circularly polarized lights (left or right-handed polarized light) by the absorbance along with the wavelength, making *g*-factor independent of sample thickness, concentration and molecular weight.<sup>[20c]</sup> More importantly, *g*-factor is proportional to the magnetic transition dipole moment ( $\hat{M}_{(Mag. dipole)}$ ) but inversely proportional to the electric transition dipole moment ( $\hat{M}_{(elec. dipole)}$ ).<sup>[20a]</sup> As shown in **Figure S20**, (CIMBA)<sub>2</sub>PbI<sub>4</sub> and (BrMBA)<sub>2</sub>PbI<sub>4</sub> series exhibit the largest *g*-factor values about  $3.1 \times 10^{-3}$  and  $2.2 \times 10^{-3}$  among all investigated HOIPs, respectively. On the other hand, the (FMBA)<sub>2</sub>PbI<sub>4</sub> series exhibit the smallest *g*-factor values of  $3.0 \times 10^{-4}$ , which is an order of magnitude smaller than that of (CIMBA)<sub>2</sub>PbI<sub>4</sub> series. Together with the observations in absorption spectra where similar  $\hat{M}_{(elec. dipole)}$  has been confirmed (vide supra), it is unambiguous to conclude the larger  $\hat{M}_{(Mag. dipole)}$  in (CIMBA)<sub>2</sub>PbI<sub>4</sub> and (BrMBA)<sub>2</sub>PbI<sub>4</sub> series among the title HOIPs. In yet another approach, CPL spectra of the fabricated films are also recorded in **Figure 3b-e** and **Figure S21**. The results clearly indicate that the Cl-substituted HOIPs exhibit the strongest CPL intensities, whereas the F-substituted ones show the lowest CPL intensities, revealing the consistent chiroptical properties of the films from the emission's perspective.

The photophysical properties and the transition dipole moments were estimated theoretically to gain more insight into the chiral perovskites as tabulated in **Table S1**. The fitted lifetimes and the

## RESEARCH ARTICLE

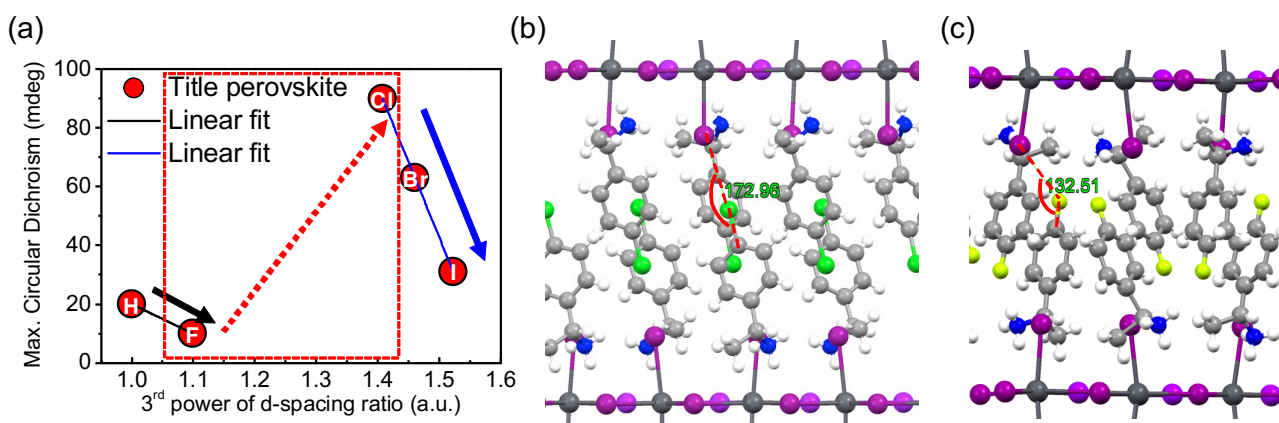


**Figure 4.** (a) Plots of the  $g$  value of CPL spectra at 535 nm (emission wavelength) versus the 3<sup>rd</sup> power of d-spacing of HOIPs. Herein, the black line represents a linear regression for (MBA)<sub>2</sub>PbI<sub>4</sub> and (FMBA)<sub>2</sub>PbI<sub>4</sub>. Also, the blue line corresponds to one with  $r^2 = 0.9957$  for (CIMBA)<sub>2</sub>PbI<sub>4</sub>, (BrMBA)<sub>2</sub>PbI<sub>4</sub> and (IMBA)<sub>2</sub>PbI<sub>4</sub> series. The red dashed square indicates the region of a significantly enhanced halogen-halogen interaction. Crystal structure of (b) Cl-substituted and (c) F-substituted chiral perovskite, where dark gray, purple, green, yellow, blue, light gray, and white balls represent Pb, I, Cl, F, N, C and H atoms, respectively.

PLQYs were recorded and employed to calculate the radiative rate constants and the electronic transition dipole moments of the perovskite films. The calculated radiative rate constants are ranging from  $3.18 \times 10^7$  to  $4.53 \times 10^7$  (s<sup>-1</sup>) for all the films, which are similar with the reported perovskite systems ( $6.2 \times 10^7$  s<sup>-1</sup>).<sup>[25]</sup> Meanwhile, the calculated electronic transition dipole moments show no obvious variance in the MBA perovskite system, affirming the experimental observation in absorption coefficient (vide supra). Additionally,  $g_{\text{PL}}$  values and the calculated electric transition dipole moments were employed to estimate the magnetic transition dipole moments.<sup>[25-26]</sup> The estimated magnetic transition dipole moments show the trend of  $1.43 \times 10^{-1} \mu_{\text{B}}$  ((CIMBA)<sub>2</sub>PbI<sub>4</sub>) >  $9.58 \times 10^{-2} \mu_{\text{B}}$  ((BrMBA)<sub>2</sub>PbI<sub>4</sub>) >  $6.33 \times 10^{-2} \mu_{\text{B}}$  ((IMBA)<sub>2</sub>PbI<sub>4</sub>) >  $2.42 \times 10^{-2} \mu_{\text{B}}$  ((MBA)<sub>2</sub>PbI<sub>4</sub>) >  $1.17 \times 10^{-2} \mu_{\text{B}}$  ((FMBA)<sub>2</sub>PbI<sub>4</sub>), where  $\mu_{\text{B}}$  is the Bohr magneton, and the trend is in good agreement with our experimental results. It is worth to note that this kind of estimation in magnetic transition dipole moment make an assumption in the incident angle ( $\theta$ ) between magnetic and electric transition dipole to be 0 degree, making the results hard to be compared with different material systems.

In order to investigate whether the observed variation in CD and CPL intensities of chiral HOIPs could be ascribed to the intrinsic property of the chiral components, rotatory strength of the *R*-form chiral molecules were estimated using time-dependent density functional theory (TD-DFT) method at B3LYP/LANL2DZ level of theory (see Table S7 in Supporting Information).<sup>[20b, 27]</sup> However, the calculated rotatory strength of chiral molecule seems erratic (Table S7) and shows no apparent correspondence with the  $g_{\text{PL}}$  of HOIPs. As illustrated in Figure S33a, the observed  $g_{\text{PL}}$  of HOIPs seems irrelevant to the rotatory strength of the organic ligands, suggesting that the chiroptical properties of the HOIPs cannot be directly deduced from the optical property of chiral organic molecules. In other words, the contribution of the achiral inorganic layer cannot be ignored.

As expressed in eq. (2), the theoretical rotatory strength of a system is a product of the electric transition dipole moment and the magnetic transition dipole moment. According to the derivations summarized in the supporting information, the electric dipole matrix is associated with the difference of the electron

momentum resulted from electronic transition. Given that all HOIPs investigated in this study display comparable absorption and emission profiles with nearly identical absorption coefficients, the obtained variation in  $g_{\text{PL}}$  should originate from the magnetic transition dipole moment term. Accordingly, the magnetic dipole matrix element ( $M_{if}$ ) expressed as eq. (4) can be related to the sum of the orbital angular momentum ( $\vec{L}$ ) and the electron spin angular momentum ( $\vec{S}$ ). However, the  $\vec{L}$  and  $\vec{S}$  of the chiral HOIPs could not be determined with computational methods.

$$M_{if} = \langle i | \vec{L} + 2\vec{S} | f \rangle \quad \text{eq. (4)}$$

Since the angular momentum of a single atom is positively related to its atomic number, we decided to look for the correlation between the  $g_{\text{PL}}$  and the atomic properties of the *para*-substituents. As the atomic number increases from 1 (for H) to 53 (for I), we expect to observe a more pronounced effect of  $\vec{L}$  on  $M_{if}$ , which should lead to a higher rotatory strength. However, plotting the maxima  $g_{\text{PL}}$  versus atomic number, atomic weight, or polarizability does not result in a conclusive argument, suggesting that the theory developed for the discrete molecular system needs to be modified for application in materials (Figure S33b-d).

As the optoelectronic properties of a material are strongly associated with the packing of its molecular units in the solid-state, we hypothesize that the chiroptical properties of HOIPs may also be derived from the structural variations of HOIPs. The first structure-property relationship identified is the d-spacing effect on the  $g_{\text{PL}}$  value obtained from CPL spectra. As illustrated in Figure 4a (or see Figure S27 in Supporting Information for a plot using CD intensity), the rotatory strength (i.e.  $g$  value) of chiral HOIPs declines as the d-spacing enlarged. While the smaller CD intensity of (FMBA)<sub>2</sub>PbI<sub>4</sub> compared to (MBA)<sub>2</sub>PbI<sub>4</sub> can be rationalized by the larger d-spacing of the former, a more pronounced trend is identified in the Cl, Br, and I-series. The observed  $g_{\text{PL}}$  value is reversely proportional to the third power of d-spacing within the (CIMBA)<sub>2</sub>PbI<sub>4</sub>, (BrMBA)<sub>2</sub>PbI<sub>4</sub>, and (IMBA)<sub>2</sub>PbI<sub>4</sub> series, indicating a smaller  $\vec{M}$  (Mag. dipole) of HOIP with a larger d-spacing.

However, the abrupt increase in  $g_{\text{PL}}$  value from (FMBA)<sub>2</sub>PbI<sub>4</sub> to (CIMBA)<sub>2</sub>PbI<sub>4</sub> cannot be explained by the d-spacing differences.

## RESEARCH ARTICLE

Thus, in addition to d-spacing, there should be another structural factor that strongly affects the  $M_{ir}$  of HOIPs. As the d-spacing is a measure of the distance between inorganic layers, the relative orientation involving chiral organic cations cannot be derived from the PXRD patterns of the HOIP thin film. Therefore, single crystals of (FMBA)<sub>2</sub>PbI<sub>4</sub> and (CIMBA)<sub>2</sub>PbI<sub>4</sub> were obtained, and their structural differences are scrutinized. The most obvious structural difference observed in (CIMBA)<sub>2</sub>PbI<sub>4</sub> is the alignment of the chiral ammonium ion with the inorganic layer through the interaction of the *para*-chlorine atom and the axial iodine of the [PbI<sub>4</sub>]<sup>2-</sup> layer with a C-Cl-I angle of around 173° (Figure 4b). However, the related C-F-I angle of 132° (similar to C-H-I angle of 134° in (MBA)<sub>2</sub>PbI<sub>4</sub> as demonstrated in Figure S16) significantly deviates from linearity, implying the lack of halogen-halogen interaction in (FMBA)<sub>2</sub>PbI<sub>4</sub> (Figure 4c). Such interaction would help fix the relative orientation of chiral molecules,<sup>[28]</sup> leading to a more regular structure and a stronger overall angular momentum for the whole material.

In short, our results indicate that the  $\hat{M}$  (*Mag. dipole*) term of the rotatory strength of HOIPs could be harnessed by interplaying the d-spacing and the halogen-halogen interaction. As the d-spacing enlargement from H to I leads the reduced rotatory strength in HOIPs, the introduction of heavy atom at the *para*-position of the phenyl group of MBA is in favor of halogen-halogen interaction. Eventually, these offsetting effects lead to the optimal CD and CPL intensity with chlorine substitution, rendering the rotatory strength and hence trend of circular dichroism intensity of the title HOIPs in order of (CIMBA)<sub>2</sub>PbI<sub>4</sub>>(BrMBA)<sub>2</sub>PbI<sub>4</sub>>(IMBA)<sub>2</sub>PbI<sub>4</sub>>(MBA)<sub>2</sub>PbI<sub>4</sub>>(FMBA)<sub>2</sub>PbI<sub>4</sub>.

## Conclusion

In summary, we have explored the chiroptical properties of a series of chiral HOIPs by incorporating chiral ammonium cations with different *para*-substituent at the phenyl ring of MBA. Varying the *para*-substituent from hydrogen to halogen atoms leads to markedly modulation in the CD and CPL intensities. The Cl-substituted HOIPs exhibit the strongest CD intensity among the chiral organic cations investigated, whereas the F-substituted ones feature the weakest CD response. The observed CD intensity is found to be generally associated with the d-spacing of HOIPs, where the increase in d-spacing will lead to a decrease in rotatory strength. However, the strong halogen-halogen interaction in Cl-substituted system leads to a dramatically enhanced rotational strength. As a result, the Cl-substituted HOIPs with the optimal angular momentum and d-spacing exhibit the highest magnetic transition dipole and display the highest rotational strength among the fabricated HOIPs. Thus, the modulation of the magnetic transition dipoles of HOIPs can be utilized for further designing the spintronic devices with high-performance chiroptical properties.

## Associated Content

**Supporting Information.** The supporting information is available free of charge via the Internet. Synthetic methods for chiral

organic cations and perovskite films are provided. Also, the corresponding characteristic analysis and computer calculation are included.

## Acknowledgements

This research was supported by the Ministry of Science and Technology of Taiwan (MOST-109-2124-M-002-011; MOST-109-2639-M-002-001-ASP).

## Conflict of interest

The authors declare no conflict of interest.

**Keywords:** Chiral • Perovskite • Rotatory strength • Circular dichroism • Circular polarized luminescence

## References

- [1] S. D. Stranks, G. E. Eperon, G. Grancini, C. Menelaou, M. J. P. Alcocer, T. Leijtens, L. M. Herz, A. Petrozza, H. J. Snaith, *Science* **2013**, *342*, 341.
- [2] a) C. C. Homes, T. Vogt, S. M. Shapiro, S. Wakimoto, A. P. Ramirez, *Science* **2001**, *293*, 673-676; b) J.-T. Lin, C.-C. Liao, C.-S. Hsu, D.-G. Chen, H.-M. Chen, M.-K. Tsai, P.-T. Chou, C.-W. Chiu, *J. Am. Chem. Soc.* **2019**, *141*, 10324-10330.
- [3] a) J.-T. Lin, D.-G. Chen, C.-H. Wu, C.-S. Hsu, C.-Y. Chien, H.-M. Chen, P.-T. Chou, C.-W. Chiu, *Angew. Chem. Int. Ed.* **2021**, *60*, 7866-7872; b) H. Huang, J. Raith, S. V. Kershaw, S. Kalytchuk, O. Tomanec, L. Jing, A. S. Susha, R. Zboril, A. L. Rogach, *Nat. Commun.* **2017**, *8*, 996; c) M. R. Filip, G. E. Eperon, H. J. Snaith, F. Giustino, *Nat. Commun.* **2014**, *5*, 5757.
- [4] a) Y. Dou, M. Wang, J. Zhang, H. Xu, B. Hu, *Adv. Funct. Mater.* **2020**, *30*, 2003476; b) M. A. Green, A. Ho-Baillie, H. J. Snaith, *Nat. Photonics* **2014**, *8*, 506-514; c) J.-T. Lin, T.-C. Chu, D.-G. Chen, Z.-X. Huang, H.-C. Chen, C.-S. Li, C.-I. Wu, P.-T. Chou, C.-W. Chiu, H. M. Chen, *ACS Appl. Energy Mater.* **2021**, *4*, 2041-2048.
- [5] a) C. Bi, Z. Yao, X. Sun, X. Wei, J. Wang, J. Tian, *Adv. Mater.* **2021**, *n/a*, 2006722; b) Y. He, J. Yan, L. Xu, B. Zhang, Q. Cheng, Y. Cao, J. Zhang, C. Tao, Y. Wei, K. Wen, Z. Kuang, G. M. Chow, Z. Shen, Q. Peng, W. Huang, J. Wang, *Adv. Mater.* **2021**, *n/a*, 2006302; c) J. Song, J. Li, X. Li, L. Xu, Y. Dong, H. Zeng, *Adv. Mater.* **2015**, *27*, 7162-7167; d) Z. Xiao, R. A. Kerner, L. Zhao, N. L. Tran, K. M. Lee, T.-W. Koh, G. D. Scholes, B. P. Rand, *Nat. Photonics* **2017**, *11*, 108-115; e) Y. Cao, N. Wang, H. Tian, J. Guo, Y. Wei, H. Chen, Y. Miao, W. Zou, K. Pan, Y. He, H. Cao, Y. Ke, M. Xu, Y. Wang, M. Yang, K. Du, Z. Fu, D. Kong, D. Dai, Y. Jin, G. Li, H. Li, Q. Peng, J. Wang, W. Huang, *Nature* **2018**, *562*, 249-253; f) Z.-K. Tan, R. S. Moggaddam, M. L. Lai, P. Docampo, R. Higler, F. Deschler, M. Price, A. Sadhanala, L. M. Pazos, D. Credgington, F. Hanusch, T. Bein, H. J. Snaith, R. H. Friend, *Nat. Nanotechnol.* **2014**, *9*, 687-692.
- [6] a) N. D. Canicoba, N. Zagni, F. Liu, G. McCuistian, K. Fernando, H. Bellezza, B. Traoré, R. Rogel, H. Tsai, L. Le Brizoual, W. Nie, J. J. Crochet, S. Tretiak, C. Katan, J. Even, M. G. Kanatzidis, B. W. Alphenaar, J.-C. Blancon, M. A. Alam, A. D. Mohite, *ACS Mater. Lett.* **2019**, *1*, 633-640; b) W. Yu, F. Li, L. Yu, M. R. Niazi, Y. Zou, D. Corzo, A. Basu, C. Ma, S. Dey,

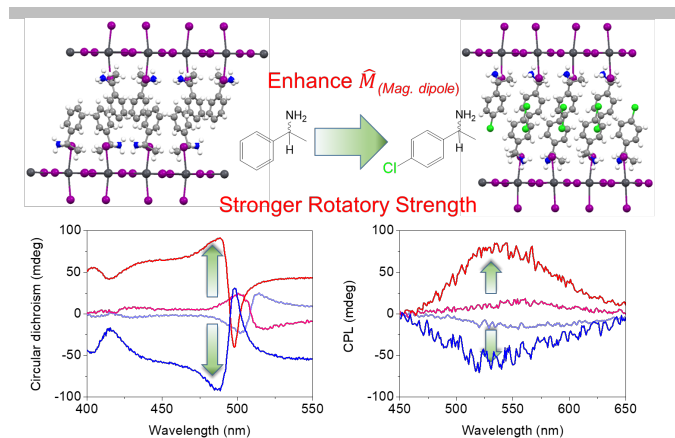
## RESEARCH ARTICLE

- M. L. Tietze, U. Buttner, X. Wang, Z. Wang, M. N. Hedhili, C. Guo, T. Wu, A. Amassian, *Nat. Commun.* **2018**, *9*, 5354; c) S. P. Senanayak, M. Abdi-Jalebi, V. S. Kamboj, R. Carey, R. Shivanna, T. Tian, G. Schweicher, J. Wang, N. Giesbrecht, D. Di Nuzzo, H. E. Beere, P. Docampo, D. A. Ritchie, D. Fairen-Jimenez, R. H. Friend, H. Sirringhaus, *Sci. Adv.* **2020**, *6*, eaaz4948.
- [7] a) J. Even, L. Pedesseau, J.-M. Jancu, C. Katan, *J. Phys. Chem. Lett.* **2013**, *4*, 2999-3005; b) A. Amat, E. Mosconi, E. Ronca, C. Quarti, P. Umari, M. K. Nazeeruddin, M. Grätzel, F. De Angelis, *Nano Lett.* **2014**, *14*, 3608-3616.
- [8] a) L. Zhang, X. Zhang, G. Lu, *J. Phys. Chem. Lett.* **2020**, *11*, 6982-6989; b) Y. Zhai, S. Baniya, C. Zhang, J. Li, P. Haney, C.-X. Sheng, E. Ehrenfreund, Z. V. Vardeny, *Sci. Adv.* **2017**, *3*, e1700704.
- [9] a) Y. Song, R. Peng, D. K. Hensley, P. V. Bonnesen, L. Liang, Z. Wu, H. M. Meyer, M. Chi, C. Ma, B. G. Sumpter, A. J. Rondinone, *ChemistrySelect* **2016**, *1*, 1-8; b) G. Long, C. Jiang, R. Sabatini, Z. Yang, M. Wei, L. N. Quan, Q. Liang, A. Rasmitha, M. Askerka, G. Walters, X. Gong, J. Xing, X. Wen, R. Quintero-Bermudez, H. Yuan, G. Xing, X. R. Wang, D. Song, O. Voznyy, M. Zhang, S. Hoogland, W. Gao, Q. Xiong, E. H. Sargent, *Nat. Photonics* **2018**, *12*, 528-533.
- [10] a) R. Naaman, Y. Paltiel, D. H. Waldeck, *Acc. Chem. Res.* **2020**, *53*, 2659-2667; b) R. Naaman, Y. Paltiel, D. H. Waldeck, *Nat. Rev. Chem.* **2019**, *3*, 250-260.
- [11] G. Long, R. Sabatini, M. I. Saidaminov, G. Lakhwani, A. Rasmitha, X. Liu, E. H. Sargent, W. Gao, *Nat. Rev. Mater.* **2020**, *5*, 423-439.
- [12] R. C. Hilborn, *Am. J. Phys.* **1982**, *50*, 982-986.
- [13] S. Han, M. Li, Y. Liu, W. Guo, M.-C. Hong, Z. Sun, J. Luo, *Nat. Commun.* **2021**, *12*, 284.
- [14] a) L. Wang, Y. Xue, M. Cui, Y. Huang, H. Xu, C. Qin, J. Yang, H. Dai, M. Yuan, *Angew. Chem. Int. Ed.* **2020**, *59*, 6442-6450; b) J. Ma, C. Fang, C. Chen, L. Jin, J. Wang, S. Wang, J. Tang, D. Li, *ACS Nano* **2019**, *13*, 3659-3665; c) H. Lu, C. Xiao, R. Song, T. Li, A. E. Maughan, A. Levin, R. Brunucky, J. J. Berry, D. B. Mitzi, V. Blum, M. C. Beard, *J. Am. Chem. Soc.* **2020**, *142*, 13030-13040; d) D. Li, X. Liu, W. Wu, Y. Peng, S. Zhao, L. Li, M. Hong, J. Luo, *Angew. Chem. Int. Ed.* **2020**, *n/a*; e) Y.-L. Zeng, X.-Q. Huang, C.-R. Huang, H. Zhang, F. Wang, Z.-X. Wang, *Angew. Chem. Int. Ed.* **2021**, *n/a*; f) Y. Dong, Y. Zhang, X. Li, Y. Feng, H. Zhang, J. Xu, *Small* **2019**, *15*, 1902237.
- [15] D. G. Billing, A. Lemmerer, *CrystEngComm* **2006**, *8*, 686-695.
- [16] J. Ahn, E. Lee, J. Tan, W. Yang, B. Kim, J. Moon, *Mater. Horiz.* **2017**, *4*, 851-856.
- [17] J. Ahn, S. Ma, J.-Y. Kim, J. Kyhm, W. Yang, J. A. Lim, N. A. Kotov, J. Moon, *J. Am. Chem. Soc.* **2020**, *142*, 4206-4212.
- [18] B. Sun, X.-F. Liu, X.-Y. Li, Y. Zhang, X. Shao, D. Yang, H.-L. Zhang, *Chem. Mater.* **2020**, *32*, 8914-8920.
- [19] R. Wang, S. Hu, X. Yang, X. Yan, H. Li, C. Sheng, *J. Mater. Chem. C* **2018**, *6*, 2989-2995.
- [20] a) N. Berova, K. Nakanishi, R. Woody, *Circular Dichroism. Principles and Applications 2nd Edition*, **2000**; b) J. A. Schellman, *Chem. Rev.* **1975**, *75*, 323-331; c) B. R. Baker, R. L. Garrell, *Faraday Discuss.* **2004**, *126*, 209-222.
- [21] Y. Nagata, T. Mori, *Front. Chem.* **2020**, *8*.
- [22] Y. Nakai, T. Mori, Y. Inoue, *J. Phys. Chem. A* **2012**, *116*, 7372-7385.
- [23] D. B. Mitzi, C. D. Dimitrakopoulos, L. L. Kosbar, *Chem. Mater.* **2001**, *13*, 3728-3740.
- [24] K. Tutaj, R. Szluzak, J. Starzyk, P. Wasko, W. Grudzinski, W. I. Gruszecki, R. Luchowski, *J. Photochem. Photobiol. B, Biol.* **2015**, *151*, 83-88.
- [25] D. Di Nuzzo, L. Cui, J. L. Greenfield, B. Zhao, R. H. Friend, S. C. J. Meskers, *ACS Nano* **2020**, *14*, 7610-7616.
- [26] M. S. Alias, I. Dursun, M. I. Saidaminov, E. M. Diallo, P. Mishra, T. K. Ng, O. M. Bakr, B. S. Ooi, *Opt. Express* **2016**, *24*, 16586-16594.
- [27] R. R. Gould, R. Hoffmann, *J. Am. Chem. Soc.* **1970**, *92*, 1813-1818.
- [28] C. Zhou, Y. Chu, L. Ma, Y. Zhong, C. Wang, Y. Liu, H. Zhang, B. Wang, X. Feng, X. Yu, X. Zhang, Y. Sun, X. Li, G. Zhao, *Phys. Chem. Chem. Phys.* **2020**, *22*, 17299-17305.

## RESEARCH ARTICLE

Entry for the Table of Contents (Please choose one layout)

Layout 1:



Through incorporating Cl-substituted chiral organic cations, chiroptical properties of 2D chiral perovskite can be significantly enhanced. The observed CD and CPL intensities are found to be associated with the d-spacing of HOIPs and the strength of the halogen-halogen interaction within the system. These findings can be utilized for further development of spintronic devices with high-performance chiroptical properties.

Institute and/or researcher Twitter usernames: ((optional))